Article

*Discovery Medicine* 2025; 37(203): 2895–2906
https://doi.org/10.24976/Discov.Med.202537203.242

# Investigation of Molecular Mechanisms Associated With Primary Aldosteronism Based on Transcriptome Sequencing

Heng Zhu[1,†], Qinke Li[1,†], Qi Huang[1], Chengwei Zhang[1], Meng Jia[1], Chunmei Liu[1], Qi Wu[1,*], Jinchen He[1,*]

[1]Cardiovascular Department, The Second Affiliated Hospital of Chengdu Medical College, Nuclear Industry 416 Hospital, 610051 Chengdu, Sichuan, China

*Correspondence: wuqi837157@163.com (Qi Wu); jinchenhe1122@outlook.com (Jinchen He)

[†]These authors contributed equally.

Submitted: 11 August 2025 Revised: 30 October 2025 Accepted: 4 November 2025 Published: 20 December 2025

**Background: Primary aldosteronism (PA) is a common cause of secondary hypertension. Despite considerable advances in medical sciences, the underlying molecular mechanisms of PA remain inadequately investigated. Therefore, this study aims to identify potential therapeutic targets for PA by using transcriptome sequencing, providing promising insights for early diagnosis and precise management of this condition.**

**Methods: Transcriptomic sequencing was performed on blood samples from PA patients and healthy controls. DESeq2 identified differentially expressed genes (DEGs). Weighted gene co-expression network analysis (WGCNA) of DEGs identified core module genes, which underwent functional enrichment for significant pathways and target detection. Subsequently, aldosterone-producing adenoma (APA) rat models were established. Potential targets (e.g., tuberous sclerosis complex 2 (*TSC2*)) were modulated via overexpression or shRNA interference, with effects validated physiologically, cellularly, and molecularly.**

**Results: Our analysis identified 277 DEGs and 8 functional modules. Eigengenes in the pink module exhibited the strongest association with disease clinical phenotypes. The genes within this module were significantly enriched in the mammalian target of rapamycin (mTOR) signaling pathway, with *TSC2* identified as a central hub gene, indicating its potential as a promising therapeutic target for PA. In APA rats, TSC2 overexpression significantly inhibited plasma aldosterone (ALD) increase ($p < 0.0001$) and elevated plasma renin activity (PRA) ($p < 0.001$). Furthermore, it inhibited adrenal cell proliferation ($p < 0.0001$), reduced S-phase fraction ($p < 0.0001$), decreased Ki67 ($p < 0.0001$), and increased p21 expression ($p < 0.01$). Western blot analysis revealed that TSC2 overexpression reduced the adrenal p-mTOR/mTOR ratio ($p < 0.0001$), while increasing p-eukaryotic translation initiation factor 4E-binding protein (p-4EBP)/4EBP ($p < 0.001$) in APA rats. Conversely, sh-TSC2 knockdown produced opposing patterns.**

**Conclusions: Transcriptome analysis identified *TSC2* as a promising therapeutic target for PA, which was later confirmed in rat models. *TSC2* likely alleviates PA by inhibiting mTOR pathway activation, thereby reducing abnormal adrenal cell proliferation and aldosterone secretion.**

**Keywords:** primary aldosteronism; transcriptomic sequencing; TSC2; mTOR signaling pathway; cell proliferation

## Introduction

Hypertension is a common cardiovascular disease, etiologically categorized as primary or secondary hypertension [1,2]. Primary aldosteronism (PA) is a common cause of secondary hypertension, primarily driven by aldosterone overproduction from adrenal zona glomerulosa cells, resulting in sodium retention, potassium excretion, and intravascular volume expansion, which suppresses renin activity. Clinically, this condition is manifested as hypertension accompanied by hypokalemic syndrome [3]. PA accounts for about 5–15% of all hypertension, up to 20% of refractory hypertension cases, and at least 4% of newly diagnosed hypertension in China [4], with prevalence increasing over time. Compared with primary hypertension, PA carries an increased risk of cardiovascular, cerebrovascular, and metabolic diseases [5]. Because its clinical manifestations often overlap with common hypertension, PA is often misdiagnosed or diagnosed late [6]. Therefore, early diagnosis and precise treatment are essential to ensure appropriate therapy.

The diagnosis and subtyping of PA is methodologically complex and typically requires a sequence of examinations, including screening tests, confirmatory testing, cross-sectional imaging, and adrenal venous sampling (AVS) [7]. AVS remains a gold standard for subtype classi-

fication and positioning. However, its success is limited by the adrenal vein anatomy, which complicates accurate intubation and can lead to unsuccessful sampling [8]. PA is primarily classified into two subtypes: aldosterone-producing adenoma (APA) and idiopathic hyperaldosteronism (IHA). APA accounts for approximately 35% of cases, most often presented as a single adenoma and may coexist with ipsilateral or contralateral normal adrenal tissue or nodular hyperplasia. IHA accounts for approximately 60% of PA cases and manifests as bilateral adrenal cortical hyperplasia, typically involving the globular zones with micro- to macronodular alterations.

The recommended therapeutic option differs by subtypes: APA is often managed with unilateral adrenalectomy [9], whereas IHA is usually managed with aldosterone receptor antagonists such as spironolactone or eplerenone [10]. However, these drugs can cause various adverse reactions, including the unusual increase in breast gland tissue (gynecomastia), erectile dysfunction, and reduced libido in men, and menstrual irregularities in women. Although unilateral adrenalectomy shows superior therapeutic efficacy for APA, some patients are poor surgical candidates due to advanced age or comorbidities. These limitations highlight the need for enhanced screening criteria and novel therapeutic targets to facilitate early diagnosis and precise treatment of PA.

Advances in molecular biology and transcriptomics analysis have become a central approach for exploring disease mechanisms and identifying potential therapeutic targets. This study aimed to identify potential therapeutic targets associated with aldosteronism by conducting transcriptome sequencing of plasma samples from patients with PA and adrenal sarcoidosis, alongside healthy controls. In combination with bioinformatics analysis, the present research also attempted to provide a theoretical basis for early screening and precise management of PA.

## Materials and Methods

### *Transcriptome Sequencing*

Peripheral blood samples were collected from patients with PA and suprarenal (adrenal) sarcoidosis (N = 10) and from healthy controls (N = 11) at the Nuclear Industry 416 Hospital. Informed consent was obtained from all participants before enrolling in the study. The study adhered to the principles outlined in the Declaration of Helsinki and received ethical approval from the hospital's ethics committee (Approval No.: YJ-2025-005-01).

Total RNA was extracted using the Trizol reagent (Item No.: 15596018, Invitrogen, USA), and RNA purity and concentration were determined using a NanoDrop 2000 (Thermo Fisher Scientific, USA). The integrity of RNA was evaluated using an Agilent 2100/LabChip GX system, and samples meeting the pre-defined quality criteria were proceeded to library construction. mRNA was enriched with Oligo (dT) using magnetic beads and fragmented with fragmentation buffer. The cDNA double-strand was synthesized using mRNA as a template and purified, and finally, the cDNA library was constructed through polymerase chain reaction (PCR) amplification. Libraries that passed quality control were sequenced on an Illumina NovaSeq6000 (Illumina, USA) using paired-end 150 bp reads (PE150).

### *Inclusion and Exclusion Criteria*

The inclusion criteria for patient selection were as follows: (1) diagnosis consistent with the *Expert Consensus on the Diagnosis and Treatment of Primary Aldosteronism (2024 version)* [11]; (2) screening aldosterone-to-renin ratio (ARR) >38 ng/dL, and a positive result on at least one confirmatory test (saline infusion test or Captopril challenge); (3) presence of adrenal mass(es); (4) patients age ranging from 18 to 75 years. Patients were excluded as follows: (1) primary hypertension or other forms of secondary hypertension, such as Cushing's syndrome or pheochromocytoma; (2) pregnancy or recent abortion; (3) severe hepatic or renal dysfunction, major cardiovascular or cerebrovascular events, or other critical conditions such as severe infection or trauma.

Inclusion criteria for healthy control selection were as follows: (1) no history of hypertension, with systolic blood pressure 90–139 mmHg and diastolic blood pressure 60–89 mmHg, according to the international standards for normal blood pressure; (2) ARR <30 ng/dL; (3) normal bilateral adrenal glands with normal morphology and size, without hyperplasia, nodules, or space-occupying lesions; (4) age ranging from 18 to 75 years. The exclusion criteria for health controls included: (1) any form of hypertension, including primary and all secondary types, and (2) the same exclusions as items (2) to (3) set for the patient group.

### *Bioinformatics Analysis*

Clean Data were generated by filtering the raw data, then aligned to the reference genome to obtain Mapped Data for further bioinformatic analysis. Differentially expressed genes (DEGs) were identified using DESeq2 v1.46.0 software with gene-level count data, applying the screening criteria of fold change $\geq 1.5$ and $p$-value $< 0.01$. DEGs distributions were visualized with a volcano plot in the R package, hierarchical clustering was conducted, and changes in their expression levels were shown in heat maps.

To identify the key DEGs module, we constructed a weighted gene co-expression network using the R package "WGCNA v1.73". Candidate soft-thresholding powers (ranging from 1 to 20) were assessed with pickSoftThreshold to determine scale independence and mean connectivity; the first power achieving a scale-free index greater than 0.8 was selected as the optimal power. A co-expression network was then constructed, and modules were identified using the blockwiseModules, each assigned a different color.

For each module, Pearson correlation coefficients and *p*-values between the module eigengenes and clinical traits were calculated, with *p*-value less than 0.05 considered statistically significant. Genes from the key module were used in Gene Ontology (GO) and Kyoto Encyclopedia of Genes and Genomes (KEGG) pathway enrichment analyses. The predictive efficacy of key module genes was evaluated using receiver operating characteristic (ROC) analysis in R, and the area under the curve (AUC) was calculated; an AUC value greater than 0.7 indicates a satisfactory predictive performance.

### *Animal Modeling, Group Treatment, and Sample Collection*

Healthy male SD rats (n = 48; aged 7 weeks and weighing 230–250 g) were obtained from Chongqing Ensiweier Biotechnology Co., Ltd. These rats were housed under controlled conditions (23 ± 2 °C, 35–60% relative humidity, and 12 h light/12 h dark cycle), with free access to food and water. Procedures involving animals were performed in strict compliance with the *Regulations on the Management of Laboratory Animals* and were approved by the Ethics Committee of the Nuclear Industry 416 Hospital (Approval No.: DWSY-2025-016) to ensure that the experimental process complies with animal welfare and ethical norms.

After a one-week acclimation, rats were randomly assigned to 8 groups, with 6 rats per group. All rats were anesthetized by intraperitoneal injection of 3% pentobarbital sodium (90 mg/kg) and implanted with a micro-osmotic pump (Item No.: 1004W, Manufacturer: Alzet, USA) for a 4-week infusion. A pump was used to infuse either a blank solvent or an aldosterone solution (Item No.: S30644, Manufacturer: OriLeaf Bio, Shanghai, China) at a rate of 1 µg/h, and was replaced once after 4 weeks [12]. Surgical procedures were performed as follows: the interscapular skin was disinfected and an incision of about 1.5 cm in length was made; the subcutaneous space was bluntly dissected with vascular forceps, a micro-osmolar pump was inserted, and the incision was then sutured. Postoperatively, penicillin (40,000 units, intramuscular) was administered daily for 3 consecutive days to prevent infection.

Furthermore, we constructed tuberous sclerosis complex 2 (TSC2) overexpression (Item No.: BR618, Fenghui Bio, Hunan, China) and knockdown (Item No.: BR698, Fenghui Bio, Hunan, China) vectors, along with their corresponding empty plasmids, and transfected them into rat adrenal cortex cells (Item NO.: CP-R236, Pricella, Wuhan, China) to evaluate transfection efficiency (**Supplementary Fig. 1**). The shRNA sequence used was: GGCAGACAATGGAAGGCATATTACTCGAGTAATATGCCTTCCATTGTCTGTTTTTTG. For the overexpression vector, the *TSC2* coding sequence was derived from NCBI Reference Sequence: NM_001430002.1 (https://www.ncbi.nlm.nih.gov/nuccore/NM_001430002.1/). In the *in vivo* analysis, one week before modeling, rats in the model group received a tail-vein injection of adenoviral vectors expressing either overexpression or knockdown of the *TSC2* gene (100 µL/rat, 1 × $10^9$ PFU/mL/rat). These rats were then monitored for 9 weeks.

After 8 weeks, three rats from both the control and model groups were randomly selected for intraperitoneal anesthesia, and blood samples were collected through inferior vena cava puncture. Plasma aldosterone (ALD) levels were measured using a rat ALD enzyme-linked immunoassay (ELISA) kit (Item No.: CB10708-Ra, Coibo Bio, Shanghai, China) to confirm the successful establishment of the APA model. After verification, all remaining rats were euthanized with intraperitoneal sodium pentobarbital (200 mg/kg), and blood samples and adrenal tissues were collected for subsequent analysis.

### *Radioimmunoassay Detection of Plasma ALD and Plasma Renin Activity (PRA) Content*

Plasma ALD and PRA were assessed using radioimmunoassay. Samples were collected as follows: For ALD, 1.5 mL of venous blood was obtained in a tube containing 0.1 mL heparin anticoagulant and stored at –80 °C. For PRA, 2 mL of venous blood was drawn into a tube containing 30 µL 3 mol/L ethylenediaminetetraacetic acid, 15 µL 0.32 mol/L dimercaptopropanol, and 30 µL 0.34 mol/L 8-hydroxyquinoline sulfate; samples were mixed and centrifuged at 2000 r/min for 5 min to isolate plasma. The aldosterone radioimmunoassay kit (Item No.: RVR-CW-100, Beijing North Institute of Biotechnology, Beijing, China) and the angiotensin I radioimmunoassay kit (Item No. KIPB3518, Beijing North Institute of Biotechnology, Beijing, China) were used to detect the plasma ALD and PRA content in each group of rats, respectively.

### *Western Blot Analysis*

Expression levels of TSC2, mammalian target of rapamycin (mTOR), p-mTOR, eukaryotic translation initiation factor 4E-binding protein (4EBP), and p-4EBP proteins in rat adrenal tissues were assessed using Western blot analysis. Total protein was extracted from rat adrenal tissue samples using RIPA lysate (Item No. P0013B, Beyotime, China). For each sample, 500 µg of total protein was mixed with 5 × SDS loading buffer at a 4:1 ratio and denatured in a metal bath for 6 min. Next, a 60 µg protein sample was resolved on a 12% SDS-PAGE gel (Item No. PG212, Epizyme Biotech, China) for separation using electrophoresis and subsequently transferred to a PVDF membrane (Item No. 10600023, Amersham, Germany). The membranes were washed with TBST for 1 min, blocked with 5% skim milk at room temperature for 1 h, and then underwent an additional 3 TBST washes (each 5 minutes). Membranes were incubated overnight at 4 °C with specific primary antibodies: anti-TSC2 (1:1000, A0492, ABclonal, China), anti-p-mTOR

**Table 1. Primer sequences used in quantitative polymerase chain reaction (qPCR).**

| Primer | Sequence (5′-3′) |
|---|---|
| *TSC2*-F | AGGACAGTTTCAGAGCACGG |
| *TSC2*-R | TCTGTATTCTGCTGCGGACC |
| *mTOR*-F | GGTGGACGAGCTCTTTGTCA |
| *mTOR*-R | AGGAGCCCTAACACTCGGAT |
| *4EBP*-F | CAGCCATAGGACGCAGTGAT |
| *4EBP*-R | TACAAGGCCTGACTGCTGTG |
| *GAPDH*-F | TGGTGCTGAGTATGTCGTGG |
| *GAPDH*-R | GGCGGAGATGATGACCCTTT |

*TSC2*, tuberous sclerosis complex 2; *mTOR*, mammalian target of rapamycin; *4EBP*, 4E-binding protein; *GAPDH*, glyceraldehyde-3-phosphate dehydrogenase.

(1:1000, AP0115, ABclonal, China), anti-mTOR (1:1000, A2445, ABclonal, China), anti-p-4EBP (1:1000, AP0344, ABclonal, China), anti-4EBP (1:1000, A24691, ABclonal, China), and anti-glyceraldehyde-3-phosphate dehydrogenase (GAPDH) (1:1000, A19056, ABclonal, China). The next day, the membranes were washed with TBST buffer 3 times (10 min each), then incubated with an horseradish peroxidase (HRP)-conjugated secondary antibody (1:2000, AS014, ABclonal, China) for 1 h at room temperature.

Finally, protein bands were developed using an enhanced chemiluminescence (ECL) kit (Item No. 34580, Thermo, USA), and images were acquired using a nucleic acid protein gel imaging system (Universal Hood II, Bio-Rad, USA). GAPDH was used as an endogenous control. Relative expression was quantified with ImageJ software and compared among different groups.

### *Quantitative Polymerase Chain Reaction (qPCR)*

Total RNA was extracted from rat adrenal tissues using Trizol reagent, and RNA quantification and purity were evaluated using a NanoDrop One (Thermo, USA). RNA was reverse transcribed into cDNA using Goldenstar™ RT6 cDNA synthesis kit (TSK302M, Tsingke, Beijing) under the following thermal conditions: 25 °C for 10 min, 55 °C for 15 min, 85 °C for 5 min, and finally stored at 4 °C. Quantitative real-time fluorescence PCR was performed using 2 × T5 Fast qPCR Mix (SYBR Green I) (TSE202, Tsingke, Beijing), with thermocycler conditions set as follows: predenaturation at 95 °C for 30 s, followed by 40 cycles of 95 °C 5s and 60 °C 30s. Fluorescence was detected on the Bio-Rad iQ5 system, and relative expression levels were determined using the $2^{-\Delta\Delta Ct}$ method. The GAPDH gene was used as the internal reference control. A list of primers used in qPCR is presented in Table 1.

### *Immunohistochemistry*

Immunohistochemistry was conducted to assess the expression and localization of Ki67 and p21 in rat adrenal tissue. Paraffin sections were dewaxed, followed by antigen retrieval by boiling for 30 min, and incubated with 3% hydrogen peroxide for 15 min at room temperature to block endogenous peroxidase. Non-specific binding was blocked with goat serum for 1 h. Tissue sections were then incubated overnight at 4 °C with rabbit monoclonal antibody to p21 (1:100, A19094, ABclonal) and Ki67 (1:100, A20018, ABclonal). After 3 three 5-minute PBS washes, sections were incubated with HRP-labeled goat anti-rabbit IgG secondary antibody (1:500, GB23303, Servicebio) for 1.5 h at room temperature, followed by 3 additional PBS washes (5 min each). Signals were developed using DAB (ZLI-9019, ZSGB-BIO) for 1 min in the dark, then counterstained with hematoxylin (G1004, Servicebio), differentiated with 1% hydrochloric acid for 2 s, and then washed for 10 min. Finally, the sections were dehydrated with gradient ethanol, cleared in xylene, sealed with neutral resin, and images were acquired using an Mshot MF53 inverted microscope.

### *Flow Cytometry Detection of the Cell Cycle*

Cell cycle status in adrenal tissues was evaluated using the Flow Cycle Kit (Item No.: AC12L543, LIFE iLAB BIO, China). Briefly, adrenal tissues were placed in pre-cooled DPBS (Item No. C0221D, Beyotime, China), minced, and washed 3 times. Tissue fragments were transferred to a 15 mL tube, centrifuged at 1000 g for 5 min at 4 °C, and the supernatant was discarded. The samples were added with 2 mg/mL of type I collagenase (Item No.: ST2294, Beyotime, China), mixed well, and heated at 37 °C in a water bath for 20 min. After centrifugation, DPBS was added to gently blow the tissue and filtered through a 200-mesh screen to remove residual tissue, and the cells were centrifuged again to obtain cell precipitation. Cells were washed 2 times with pre-cooled PBS and centrifuged at 2000 rpm for 5 min, then fixed with 1 mL of 70% ethanol at 4 °C for 24 h. Immobilized cells were washed twice with PBS, resuspended in about 50 µL of PBS, and dispersed by gentle tapping. Propidium iodide staining solution (0.5 mL) was added, and cells were incubated at 37 °C for 30 minutes in the dark, and then stored at 4 °C. Finally, red fluorescence and light scatter were detected at an excitation wavelength of 488 nm using a flow cytometer (CytoFLEX, Beckman, USA).

### *5-Ethynyl-2′-deoxyuridine (EdU) Staining*

Cell proliferation in adrenal tissue was evaluated using the BeyoClick™ EdU-555 Cell Proliferation Assay Kit (Item No. C0075S, Beyotime, China). Paraffin sections were routinely dewaxed and rehydrated, followed by subsequent staining. Approximately 100 µL of Click reaction solution was added to each section and incubated for 30 minutes at room temperature in the dark, followed by 3 PBS washes (5 min each). In the next step, nuclei were counterstained with DAPI (Item No. C1005, Beyotime, China) for 5 min in the dark and then washed 3 times with PBS (5 min each) to remove excess dye. Finally, sections were mounted

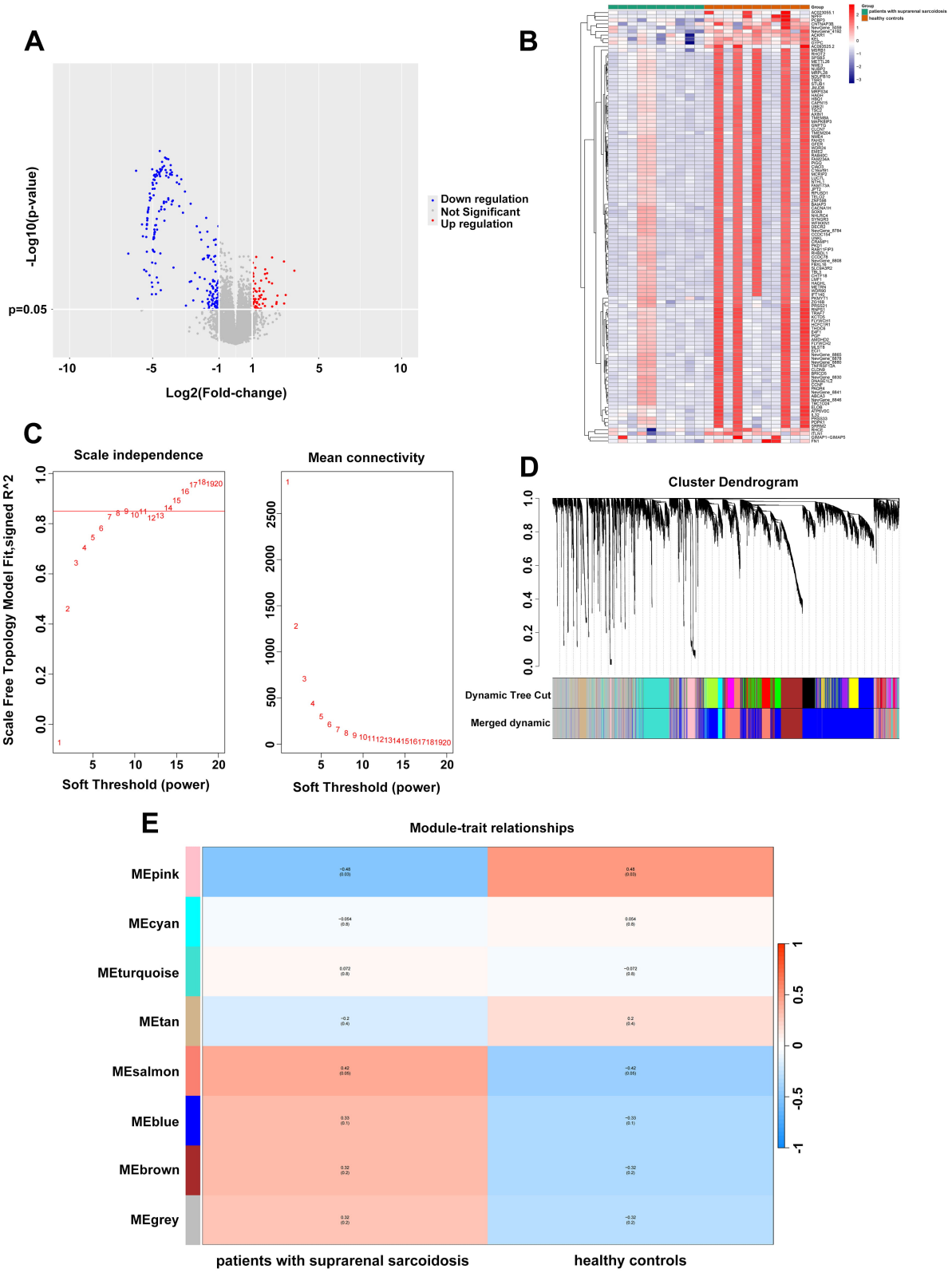


**Fig. 1. Differential expression analysis and weighted gene co-expression network analysis (WGCNA) analysis between the patient and control groups.** (A) Volcano plots of the differentially expressed genes (DEGs). (B) Cluster heatmap of the DEGs. (C) Network topology for different soft thresholding powers (ranging from 1 to 20). The scale-free topology can be attained at the soft-power of 8. (D) Cluster dendrogram and gene modules identified by WGCNA analysis. (E) Visualization of the relationships between modules and traits via a heatmap, labelled with correlation coefficient and *p*-value.

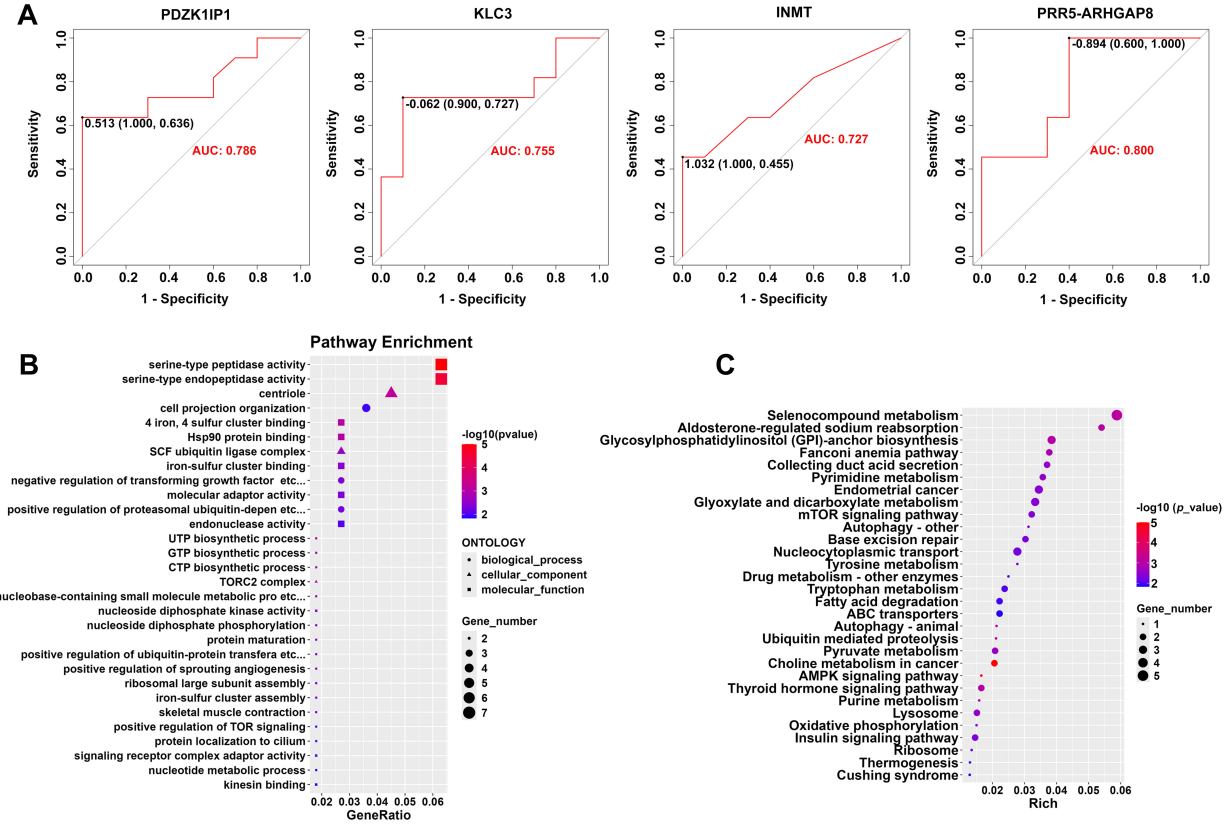


**Fig. 2. Screening of potential biomarkers for adrenal nodules and functional enrichment analysis of key module genes.** (A) Receiver operating characteristic (ROC) analysis for potential biomarkers based on the pink module. The optimal cutoff values "0.513", "–0.062", "1.032", and "–0.894" in Fig. 2A are presented on the log-odds scale (linear predictor), which is commonly used in logistic regression models. When the event probability is less than 1.0, both the odds ratio and the log-odds will be negative. The values in parentheses correspond to the diagnostic performance at each cutoff, presented as (Specificity, Sensitivity). (B) Gene Ontology (GO) enrichment analysis of the pink module genes. (C) Enriched Kyoto Encyclopedia of Genes and Genomes (KEGG) pathways in the pink module genes.

with anti-fluorescence quencher (Item No.: P0126, Beyotime, China) and examined using an Mshot MF53 inverted microscope.

### *Statistical Analysis*

Data were expressed as mean ± standard error. For normally distributed variables, multiple groups were performed using one-way analysis of variance (ANOVA) followed by Tukey's post hoc test, whereas the Friedman test was applied to non-normally distributed variables. Statistical analysis and plotting were performed in GraphPad Prism 8 software (Dotmatics, USA), and $p < 0.05$ was considered statistically significant.

## Results

### *Identification of DEGs and Module Eigengenes*

Volcanogram results (volcano plot analysis) identified 277 DEGs between patients and controls (Fig. 1A). The cluster heatmap analysis revealed sample-wise expression patterns of these DEGs (Fig. 1B). Weighted gene co-expression network analysis (WGCNA) analysis was then applied to the DEG sets between the two groups. Using a soft threshold power of 8 (Fig. 1C), 8 functional (co-expression) modules were identified (Fig. 1D). Among them, the *p*-value of the module eigengenes located in the pink module was 0.03, which was identified as key module genes (Fig. 1E), indicating that it had the highest correlation with the clinical characteristics of the suprarenal nodule.

### *Function Enrichment Analysis*

Using ROC analysis in the R package, the predictive performance of genes from the pink module was assessed to identify potential biomarkers for adrenal nodules. PDZK1-interacting protein 1 (PDZK1IP1), kinesin light chain 3 (KLC3), Indolethylamine N-methyltransferase (INMT), and proline rich 5, renal-Rho GTPase activating protein 8 (PRR5-ARHGAP8) demonstrated promising discrimination, with AUCs of 0.786, 0.755, 0.727, and 0.800, respectively (Fig. 2A).

To further characterize these key module genes, we performed functional and pathway enrichment analysis. GO analysis showed enrichment in cell projection organization (Biological Process), serine-type peptidase activity (Molecular Function), and the centriole (Cellular Component) (Fig. 2B). KEGG pathway enrichment analysis of key module genes (Fig. 2C) showed the mTOR signaling pathway as the most significantly enriched (smallest *p*-value). Five genes, including *TELO2*, *TSC2*, *WDR24*, *PDPK1*, and *MLST8*, were mapped to the mTOR signaling pathway. Based on the KEGG metabolic pathway map (https://www.kegg.jp/pathway/map04150), *TSC2* was found to be located at the central hub of the mTOR signaling pathway (Entry: map04150) (**Supplementary Fig. 2**). Therefore, we speculated that *TSC2* might be a potential therapeutic target in PA.

### *Validation of the Potential Role of TSC2 in an APA Rat Model*

To further explore the potential role of *TSC2* in PA, we constructed an APA rat model and administered adenoviral vectors through the tail vein to overexpress or knock down *TSC2*. Plasma ALD was significantly higher in the model group than in the control group ($p < 0.0001$), confirming that the rat model of APA was successfully constructed (Fig. 3A). TSC2 overexpression (oe-*TSC2*) significantly inhibited the ALD increase in APA rats ($p < 0.0001$) and increased PRA ($p < 0.001$) (Fig. 3B,C). In contrast, treatment with sh-*TSC2* further significantly increased ALD levels ($p < 0.01$) and notably decreased PRA ($p < 0.01$) (Fig. 4A,B).

qPCR analysis showed a substantial decrease in *TSC2* mRNA in adrenal tissue from the model group compared to the control group ($p < 0.0001$). TSC2 expression increased after oe-TSC2 treatment ($p < 0.0001$) (Fig. 3D) and decreased significantly after sh-TSC2 treatment ($p < 0.01$) (Fig. 4C). However, there was no statistical difference in mTOR and 4EBP mRNA levels between the experimental groups.

WB analysis revealed that, compared with the control group, the model group had lower TSC2 ($p < 0.0001$) and p-4EBP/4EBP ($p < 0.0001$) expression and higher p-mTOR/mTOR ($p < 0.0001$). The oe-TSC2 treatment significantly up-regulated TSC2 ($p < 0.0001$) and p-4EBP/4EBP ($p < 0.001$) expression and inhibited p-mTOR/mTOR ($p < 0.0001$) in APA rats (Fig. 3E). In contrast, sh-TSC2 treatment significantly down-regulated TSC2 ($p < 0.001$) and p-4EBP/4EBP ($p < 0.001$) expression and up-regulated p-mTOR/mTOR ($p < 0.01$, Fig. 4D).

Immunohistochemistry revealed a significant increase in Ki67 ($p < 0.0001$) and a substantial decrease in p21 ($p < 0.001$) in the model group compared to the control group. After oe-TSC2 treatment, the expression level of Ki67 was significantly reduced ($p < 0.0001$) while the expression of p21 was significantly increased ($p < 0.01$, Fig. 3F,H). In contrast, sh-TSC2 treatment resulted in a significant increase in the expression of Ki67 ($p < 0.0001$) while a significant decrease in that of p21 ($p < 0.05$, Fig. 4E,G). Furthermore, EdU staining validated these trends: oe-TSC2 treatment significantly inhibited cell proliferation in adrenal tissues of APA rats ($p < 0.0001$, Fig. 3G,I), whereas sh-TSC2 substantially promoted cell proliferation ($p < 0.001$, Fig. 4F,H).

Flow cytometry analysis of adrenal tissues revealed that oe-TSC2 substantially reduced the proportion of S-phase cells in APA rats ($p < 0.0001$, Fig. 3J, **Supplementary Fig. 3A**), whereas sh-TSC2 treatment significantly increased S-phase fraction ($p < 0.0001$, Fig. 4I, **Supplementary Fig. 3B**). These findings revealed that reduced TSC2 induces abnormal proliferation of adrenal tissue cells by modulating the mTOR signaling pathway, promoting adrenal hyperplasia and nodule formation, and ultimately contributing to PA.

## Discussion

PA, a common secondary hypertension, often presents clinical features similar to primary hypertension, leading to misdiagnosis or delayed treatment and ultimately suboptimal therapeutic outcomes. Identifying novel biomarkers and potential therapeutic targets is crucial for earlier detection and precise treatment. Through transcriptome profiling of plasma samples from patients with adrenal sarcoidosis and healthy controls, combined with bioinformatics analysis, this study aimed to uncover potential disease targets associated with aldosteronism, expecting to lay a theoretical foundation to support earlier diagnosis and personalized treatment for PA.

Transcriptome sequencing identified 277 PA-associated DEGs between groups, and WGCNA analysis showed that the pink module eigengenes were strongly correlated with the clinical characteristics of PA. Further ROC analysis revealed that certain key genes in this module, including PDZK1IP1, KLC3, INMT, and PRR5-ARHGAP8, may serve as potential disease markers for PA. For example, Li *et al.* [13] reported that KLC3 is a potential biomarker in hypertension, with significant expression differences in hypertensive patients. However, evidence correlating PDZK1IP1, INMT, and PRR5-ARHGAP8 to hypertension-related diseases remains limited.

mTOR is an atypical protein kinase in the phosphoinositide 3-kinase (PI3K) -related family, mainly consisting of two complexes, the rapamycin-sensitive mTOR complex 1 (mTORC1) and the non-rapamycin-sensitive mTOR complex 2 (mTORC2). These complexes regulate cell proliferation, survival, autophagy, metabolism, and immunity responses [14,15]. *TSC2* is a tumor suppressor gene that encodes tuberin. Tuberin forms a complex with hamartin to negatively regulate mTORC1, thereby inhibiting mTOR activation and controlling cell growth and metabolic processes [16]. Loss-of-function mutations in *TSC2* lead to

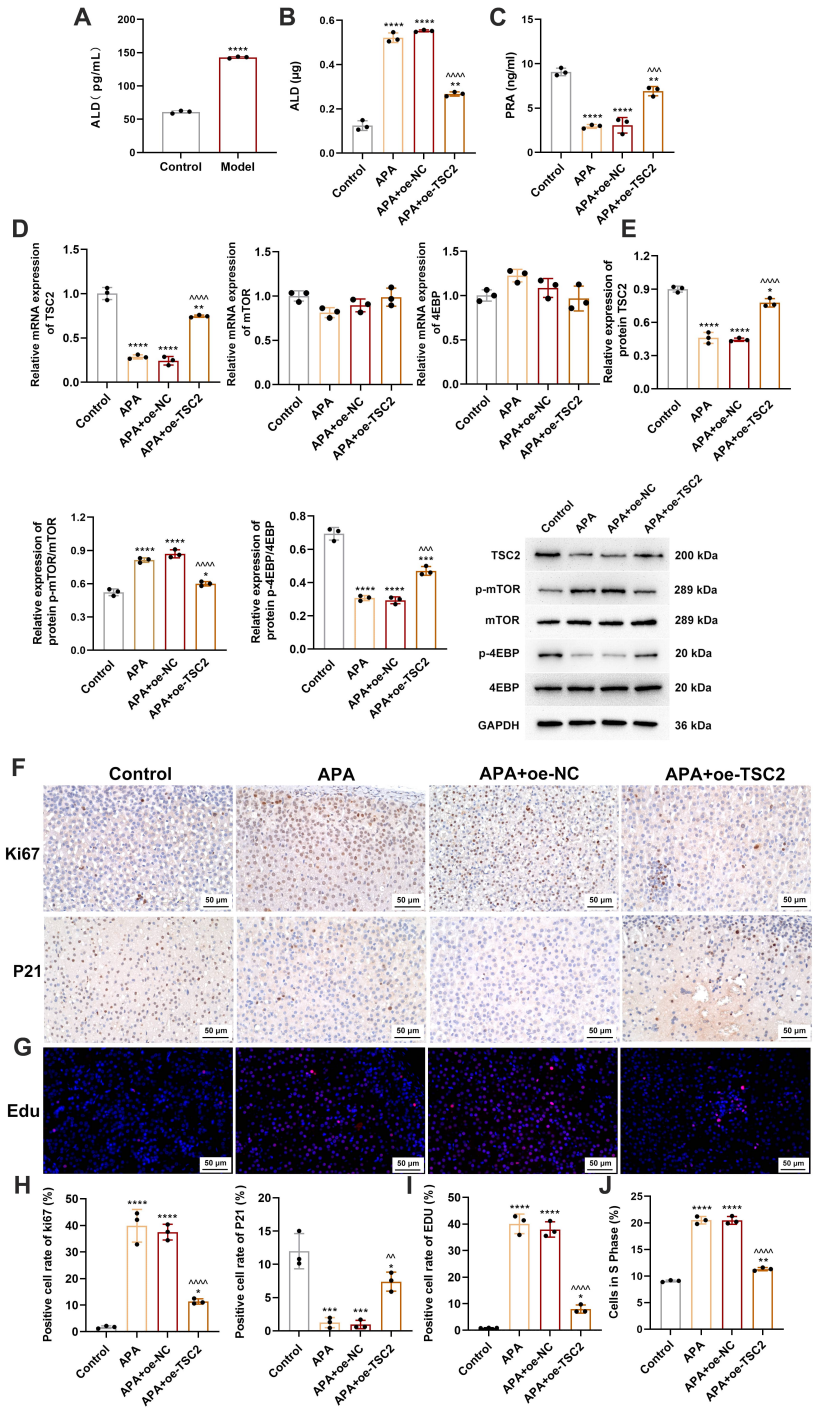


**Fig. 3. Impacts of tuberous sclerosis complex 2 (TSC2) overexpression on the aldosterone-producing adenoma (APA) rat model.** (A) Enzyme-linked immunoassay (ELISA) detection of plasma aldosterone (ALD) concentration to validate the APA rat model. (B) Radioimmunoassay detection for plasma ALD level. (C) Radioimmunoassay detection for plasma renin activity (PRA). (D) PCR detection of mRNA levels of *TSC2*, mammalian target of rapamycin (mTOR), and eukaryotic translation initiation factor 4E-binding protein (4EBP) in adrenal tissues under oe-TSC2 treatment. (E) WB analysis of protein expression levels of TSC2, p-mTOR, mTOR, p-4EBP, and 4EBP in adrenal tissues under oe-TSC2 treatment. (F,H) Immunohistochemical analysis of protein expression and localization of Ki67 and p21 in adrenal tissues under oe-TSC2 treatment. The magnification is 400× for the representative immunohistochemical images. (G,I) 5-Ethynyl-2′-deoxyuridine (EdU) staining to detect cell proliferation under oe-TSC2 treatment. The magnification is 400× for the representative EdU staining images. (J) Flow cytometry analysis of the cell cycle in adrenal tissues after oe-TSC2 treatment. Note: Compared to the Control group, * $p < 0.05$, ** $p < 0.01$, *** $p < 0.001$, and **** $p < 0.0001$; Compared to the APA group, ^^ $p < 0.01$, ^^^ $p < 0.001$, and ^^^^ $p < 0.0001$.

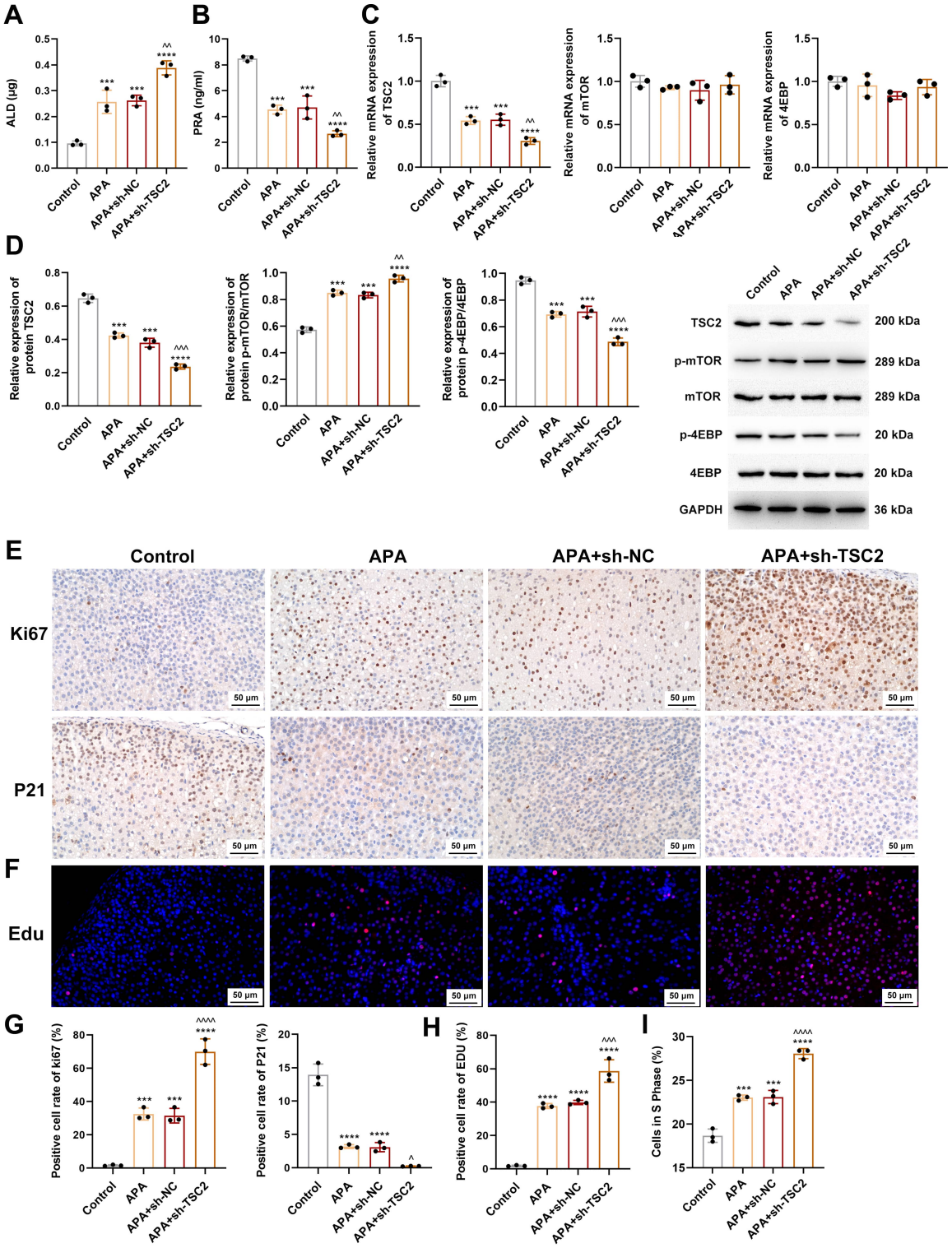


**Fig. 4. Investigation of TSC2 knockdown effects in an APA rat model.** (A) ALD levels detection. (B) PRA detection. (C) PCR detection for mRNA levels of *TSC2*, mTOR, and 4EBP in adrenal tissues under sh-TSC2 treatment. (D) WB analysis for protein expression levels of TSC2, p-mTOR, mTOR, p-4EBP, and 4EBP in adrenal tissues under sh-TSC2 treatment. (E,G) Immunohistochemical analysis of protein expression and localization of Ki67 and p21 in adrenal tissues under sh-TSC2 treatment. The magnification is 400× for the representative immunohistochemical images. (F,H) EdU staining to detect cell proliferation under sh-TSC2 treatment. (I) Flow cytometry analysis of the cell cycle in adrenal tissues under sh-TSC2 treatment. The magnification is 400× for the representative EdU staining images. Note: Compared to the Control group, *** $p < 0.001$, and **** $p < 0.0001$; Compared to the APA group, ^ $p < 0.05$, ^^ $p < 0.01$, ^^^ $p < 0.001$, and ^^^^ $p < 0.0001$.

over-activation of the mTOR pathway, leading to the disease across multiple organs, including the kidneys and nervous system [17–19]. In our study, KEGG enrichment revealed that the key module genes were significantly enriched in the mTOR signaling pathway, and *TSC2* was found to be located at the hub of the mTOR signaling pathway, indicating a crucial role for *TSC2* in PA pathogenesis via modulation of mTOR. Previous research on PA has similarly correlated the mTOR signaling pathway with aldosterone synthesis and secretion, and reported increased mTOR signaling pathway activity in affected adrenal tissue [20].

To further elucidate the role of *TSC2* in PA, we established an APA rat model and performed TSC2 overexpression and knockdown interventions. TSC2 overexpression significantly inhibited adrenal cell proliferation and reduced the S-phase fraction. Immunohistochemistry analysis further validated these findings: Ki67, a proliferation marker [21], was reduced, while p21, a cell-cycle inhibitor that prevents G1-S phase transition [22], increased. In contrast, knockdown of TSC2 produced the opposite pattern. These results reveal that *TSC2* may mitigate the progression of PA by inhibiting cell proliferation, promoting cell cycle arrest, thereby preventing adrenal hyperplasia and nodule formation.

Eukaryotic translation initiation factor 4E-binding protein 1 (4EBP1) is an inhibitory factor that suppresses translation initiation by binding to eukaryotic translation initiation factor 4E (eIF4E) [23]. Activation of mTOR enhances phosphorylation of 4EBP1, relieves its suppression of eIF4E, and promotes synthesis of ribosomal and other translation-regulated proteins, thereby participating in cell proliferation [24]. Aberrant mTOR signaling is closely associated with multiple tumors and metabolic diseases [19]. In our study, Western blot analysis revealed that TSC2 overexpression inhibited the p-mTOR/mTOR ratio and significantly increased p-4EBP/4EBP in the adrenal tissue from APA rats, whereas TSC2 silencing showed the opposite effect. These findings are consistent with previous studies: the adrenocortical carcinoma cell lines NCI-H295R, a standard aldosterone-secreting cellular model due to their aldosterone-secreting properties, demonstrated higher mTOR activity, and mTOR suppression significantly inhibited its growth and proliferation [25]. Shen *et al*. [26] have reported that *TSC2* reduces cell proliferation in other tumor types by limiting the mTOR pathway. Collectively, the findings support the model in which *TSC2* alleviates PA by inhibiting the activation of the mTOR pathway, thereby hindering the proliferation of aldosterone-producing cells and reducing the aldosterone secretion.

Despite some valuable outcomes, this study has several limitations. First, the sample size for transcriptomic analysis was relatively small, which may limit the generalizability of the identified DEGs. Second, while the APA rat model provides mechanistic insight, validation in human PA cohorts is warranted. Third, although the mTOR pathway appears crucial, other pathways and underlying molecular mechanisms are likely to be involved in PA and need confirmation in future studies. Finally, translating these findings into effective clinical interventions remains challenging and will need multi-center, prospective investigations.

## Conclusions

This study demonstrated that TSC2 is a key modulator in PA. Transcriptomic analysis highlighted its relevance, and an *in vivo* rat model verified the hypothesis. TSC2 might alleviate PA by inhibiting activation of the mTOR pathway, inhibiting abnormal proliferation of PA cells, and aldosterone secretion. These observations support TSC2 as a viable therapeutic target for PA and provide a theoretical basis for early diagnosis and more precise, targeted treatment options.

## Abbreviations

PA, primary aldosteronism; DEGs, differentially expressed genes; WGCNA, weighted gene co-expression network analysis; EdU staining, 5-Ethynyl-2′-deoxyuridine staining; APA, aldosterone-producing adenoma; ARR, aldosterone-to-renin ratio; AVS, adrenal venous sampling; IHA; idiopathic hyperaldosteronism; AUC, area under the curve; ALD, aldosterone; ELISA, enzyme-linked immunoassay assay; PRA, plasma renin activity; PI3K, phosphoinositide 3-kinase; 4EBP1, eukaryotic translation initiation factor 4E-binding protein 1; eIF4E, eukaryotic translation initiation factor 4E; TSC2, tuberous sclerosis complex 2; mTOR, mammalian target of rapamycin; GO, gene ontology; KEGG, kyoto encyclopedia of genes and genomes; ROC, receiver operating characteristic; GAPDH, glyceraldehyde-3-phosphate dehydrogenase; PCR, polymerase chain reaction; qPCR, quantitative polymerase chain reaction; ANOVA, one-way analysis of variance; mTORC1, mTOR complex 1; mTORC2, mTOR complex 2; 4EBP, eukaryotic translation initiation factor 4E-binding protein; PDZK1IP1, PDZK1-interacting protein 1; INMT, indolethylamine N-methyltransferase; KLC3, kinesin light chain 3; PRR5-ARHGAP8, proline rich 5, renal-Rho GTPase activating protein 8; HRP, horseradish peroxidase; ECL, enhanced chemiluminescence.

## Availability of Data and Materials

The datasets used and/or analyzed during the current study are available from the corresponding author on reasonable request.

## Author Contributions

HZ and QKL designed the research study, and contributed to writing the original manuscript. QH and CWZ provided human samples for transcriptomic sequencing, and involved in the experimental operation. MJ and CML were responsible for data analysis and preparing figures and the table. QW and JCH made contributions to the conception and design, acquisition of data, and analysis and interpretation of data. All authors contributed to critical revision of the manuscript for important intellectual content. All authors read and approved the final manuscript. All authors have participated sufficiently in the work and agreed to be accountable for all aspects of the work.

## Ethics Approval and Consent to Participate

All subjects provided signed informed consent before participating in this study, and the experiments were conducted in strict compliance with the relevant provisions of the Declaration of Helsinki and had been approved by the Medical Ethics Committee of the Nuclear Industry 416 Hospital (Approval No.: YJ-2025-005-01). Procedures involving animals were performed in strict compliance with the *Regulations on the Management of Laboratory Animals* and were approved by the Ethics Committee of the Nuclear Industry 416 Hospital (Approval No.: DWSY-2025-016).

## Acknowledgment

Not applicable.

## Funding

This work was supported by the Key Research and Development Project of Sichuan Provincial Science and Technology Department (grant number 24ZDYF0624); 2024 Central Government Guides Local Science and Technology Development Project (grant number 2024ZYD0091); Clinical Science Research Fund Project of Chengdu Medical College (grant number 24LHBBYY1-05); and Chengdu Clinical Key Specialty Project (grant number CDS2023ZD002).

## Conflict of Interest

The authors declare no conflict of interest.

## Supplementary Material

Supplementary material associated with this article can be found, in the online version, at https://doi.org/10.24976/Discov.Med.202537203.242.

## References

[1] Williams B, Mancia G, Spiering W, Agabiti Rosei E, Azizi M, Burnier M, *et al*. 2018 ESC/ESH Guidelines for the management of arterial hypertension. European Heart Journal. 2018; 39: 3021–3104. https://doi.org/10.1093/eurheartj/ehy339.

[2] Yihui C, Yanfeng G. Inflammatory markers in patients with hypertension. British Journal of Hospital Medicine. 2023; 84: 1–8. https://doi.org/10.12968/hmed.2022.0531.

[3] Monticone S, Burrello J, Tizzani D, Bertello C, Viola A, Buffolo F, *et al*. Prevalence and Clinical Manifestations of Primary Aldosteronism Encountered in Primary Care Practice. Journal of the American College of Cardiology. 2017; 69: 1811–1820. https://doi.org/10.1016/j.jacc.2017.01.052.

[4] Xu Z, Yang J, Hu J, Song Y, He W, Luo T, *et al*. Primary Aldosteronism in Patients in China With Recently Detected Hypertension. Journal of the American College of Cardiology. 2020; 75: 1913–1922. https://doi.org/10.1016/j.jacc.2020.02.052.

[5] Monticone S, D'Ascenzo F, Moretti C, Williams TA, Veglio F, Gaita F, *et al*. Cardiovascular events and target organ damage in primary aldosteronism compared with essential hypertension: a systematic review and meta-analysis. The Lancet. Diabetes & Endocrinology. 2018; 6: 41–50. https://doi.org/10.1016/S2213-8587(17)30319-4.

[6] Brown JM, Siddiqui M, Calhoun DA, Carey RM, Hopkins PN, Williams GH, *et al*. The Unrecognized Prevalence of Primary Aldosteronism: A Cross-sectional Study. Annals of Internal Medicine. 2020; 173: 10–20. https://doi.org/10.7326/M20-0065.

[7] Funder JW, Carey RM, Mantero F, Murad MH, Reincke M, Shibata H, *et al*. The Management of Primary Aldosteronism: Case Detection, Diagnosis, and Treatment: An Endocrine Society Clinical Practice Guideline. The Journal of Clinical Endocrinology and Metabolism. 2016; 101: 1889–1916. https://doi.org/10.1210/jc.2015-4061.

[8] Deinum J, Turcu AF. Adrenal Vein Sampling in Primary Aldosteronism-Is The Gold Standard Losing Its Luster? The Journal of Clinical Endocrinology and Metabolism. 2025; 110: e2800–e2803. https://doi.org/10.1210/clinem/dgaf204.

[9] Williams TA, Lenders JWM, Mulatero P, Burrello J, Rottenkolber M, Adolf C, *et al*. Outcomes after adrenalectomy for unilateral primary aldosteronism: an international consensus on outcome measures and analysis of remission rates in an international cohort. The Lancet. Diabetes & Endocrinology. 2017; 5: 689–699. https://doi.org/10.1016/S2213-8587(17)30135-3.

[10] Karagiannis A, Tziomalos K, Papageorgiou A, Kakafika AI, Pagourelias ED, Anagnostis P, *et al*. Spironolactone versus eplerenone for the treatment of idiopathic hyperaldosteronism. Expert Opinion on Pharmacotherapy. 2008; 9: 509–515. https://doi.org/10.1517/14656566.9.4.509.

[11] Chinese Society of Endocrinology, Chinese Medical Association (2025). Expert Consensus on the Diagnosis and Treatment of Primary Aldosteronism (2024 Edition). Chinese Journal of Endocrinology and Metabolism. 2025; 41: 12–24. (In Chinese)

[12] Yan Y, Wang C, Lu Y, Gong H, Wu Z, Ma X, *et al*. Mineralocorticoid receptor antagonism protects the aorta from vascular smooth muscle cell proliferation and collagen deposition in a rat model of adrenal aldosterone-producing adenoma. Journal of Physiology and Biochemistry. 2018; 74: 17–24. https://doi.org/10.1007/s13105-017-0600-2.

[13] Li Z, Tian L, Bai L, Jia Z, Wu X, Song C. Identification of hypertension gene expression biomarkers based on the DeepGCFS algorithm. PloS One. 2025; 20: e0314319. https://doi.org/10.1371/journal.pone.0314319.

[14] Jung S, Gámez-Díaz L, Proietti M, Grimbacher B. "Immune TOR-opathies," a Novel Disease Entity in Clinical Immunology. Frontiers in Immunology. 2018; 9: 966. https://doi.org/10.3389/fimmu.2018.00966.

[15] Chen J, Xia CL, Dong R, Liu XG, Xia J. Cepharanthine Inhibits Doxorubicin-Induced Cellular Senescence by Activat-

ing Autophagy via the mTOR Signaling Pathway. Discovery Medicine. 2023; 35: 777–786. https://doi.org/10.24976/Discov.Med.202335178.72.

[16] Huang J, Manning BD. The TSC1-TSC2 complex: a molecular switchboard controlling cell growth. The Biochemical Journal. 2008; 412: 179–190. https://doi.org/10.1042/BJ20080281.

[17] Jurca AA, Jurca AD, Petchesi CD, Bembea D, Jurca CM, Severin E, *et al*. Tuberous Sclerosis Complex: New Insights into Pathogenesis and Therapeutic Breakthroughs. Life (Basel, Switzerland). 2025; 15: 368. https://doi.org/10.3390/life15030368.

[18] Wang H, Hu D, Cheng C, Zhang X, Liu J, Tian X, *et al*. Synergistic effects of mTOR inhibitors with VEGFR3 inhibitors on the interaction between TSC2-mutated cells and lymphatic endothelial cells. Science China. Life Sciences. 2025; 68: 1676–1688. https://doi.org/10.1007/s11427-024-2760-4.

[19] Zhao S, Hao S, Zhou J, Chen X, Zhang T, Qi Z, *et al*. mTOR/miR-142-3p/PRAS40 signaling cascade is critical for tuberous sclerosis complex-associated renal cystogenesis. Cellular & Molecular Biology Letters. 2024; 29: 125. https://doi.org/10.1186/s11658-024-00638-x.

[20] Trinh B, Hepprich M, Betz MJ, Burkard T, Cavelti-Weder C, Seelig E, *et al*. Treatment of Primary Aldosteronism With mTORC1 Inhibitors. The Journal of Clinical Endocrinology and Metabolism. 2019; 104: 4703–4714. https://doi.org/10.1210/jc.2019-00563.

[21] Wang W, Liu X, Wang W, Li J, Li Y, Li L, *et al*. The Effects of Indoxyl Sulfate on Human Umbilical Cord-Derived Mesenchymal Stem Cells In Vitro. Cellular Physiology and Biochemistry: International Journal of Experimental Cellular Physiology, Biochemistry, and Pharmacology. 2016; 38: 401–414. https://doi.org/10.1159/000438639.

[22] McCluskey E, Velli SK, Kaminski R, Markward T, Leming H, Yu D, *et al*. HOXA1 Contributes to Bronchial Epithelial Cell Cycle Progression by Regulating p21/CDKN1A. International Journal of Molecular Sciences. 2025; 26: 2332. https://doi.org/10.3390/ijms26052332.

[23] Wang S, Zhang Y, Wang M, Zhai Z, Tan Y, Xu W, *et al*. Non-canonical feedback loop between “RIP3-MLKL” and “4EBP1-eIF4E” promotes neuronal necroptosis. MedComm. 2025; 6: e70107. https://doi.org/10.1002/mco2.70107.

[24] Wan X, Helman LJ. The biology behind mTOR inhibition in sarcoma. The Oncologist. 2007; 12: 1007–1018. https://doi.org/10.1634/theoncologist.12-8-1007.

[25] Doghman M, El Wakil A, Cardinaud B, Thomas E, Wang J, Zhao W, *et al*. Regulation of insulin-like growth factor-mammalian target of rapamycin signaling by microRNA in childhood adrenocortical tumors. Cancer Research. 2010; 70: 4666–4675. https://doi.org/10.1158/0008-5472.CAN-09-3970.

[26] Shen Y, Dong X, Li X, Shi Z, Shao T, Jiang J, *et al*. WNT inhibitor SP5-mediated SERPING1 suppresses lung adenocarcinoma progression via TSC2/mTOR pathway. Cell Death & Disease. 2025; 16: 103. https://doi.org/10.1038/s41419-025-07440-3.